Editors' Suggestion | Featured in Physics

Cryogenic Optical Lattice Clock with 1.7×10^{-20} Blackbody Radiation Stark Uncertainty

Youssef S. Hassan,[1,2] Kyle Beloy,[1] Jacob L. Siegel,[1,2] Takumi Kobayashi,[1,3] Eric Swiler,[1,2] Tanner Grogan,[1,2] Roger C. Brown,[1,2] Tristan Rojo,[1,2] Tobias Bothwell,[1] Benjamin D. Hunt,[1,2] Adam Halaoui,[1] and Andrew D. Ludlow[1,2,4,*]

[1]*National Institute of Standards and Technology, 325 Broadway, Boulder, Colorado 80305, USA*
[2]*Department of Physics, University of Colorado, Boulder, Colorado 80309, USA*
[3]*National Metrology Institute of Japan (NMIJ), National Institute of Advanced Industrial Science and Technology (AIST), 1-1-1 Umezono, Tsukuba, Ibaraki 305-8563, Japan*
[4]*Electrical, Computer & Energy Engineering, University of Colorado, Boulder, Colorado 80309, USA*

(Received 25 April 2025; accepted 12 June 2025; published 5 August 2025)

Controlling the Stark perturbation from ambient thermal radiation is key to advancing the performance of many atomic frequency standards, including state-of-the-art optical lattice clocks (OLCs). We demonstrate a cryogenic OLC that utilizes a dynamically actuated radiation shield to control the perturbation at 1.7×10^{-20} fractional frequency, a factor of ~40 beyond the best OLC to date. Our shield furnishes the atoms with a near-ideal cryogenic blackbody radiation (BBR) environment by rejecting external thermal radiation at the part-per-million level during clock spectroscopy, overcoming a key limitation with previous cryogenic BBR control solutions in OLCs. While the lowest BBR shift uncertainty is realized with cryogenic operation, we further exploit the radiation control that the shield offers over a wide range of temperatures to directly measure and verify the leading BBR Stark dynamic correction coefficient for ytterbium. This independent measurement reduces the literature-combined uncertainty of this coefficient by 30%, thus benefiting state-of-the-art Yb OLCs operated at room temperature. We verify the static BBR coefficient for Yb at the low 10^{-18} level.

DOI: 10.1103/4tky-jmsm

Thermal radiation is ubiquitous in nature, inescapable even in outer space. An ideal blackbody radiation (BBR) environment—characteristic of isothermal surroundings—is homogeneous, isotropic, spectrally Planckian, and characterized exclusively by its temperature. In atomic clocks, this thermal radiation perturbs the atomic energy levels, inducing a Stark shift to the clock frequency conventionally known as the BBR shift. For over four decades, the BBR shift has been a persistent challenge in the pursuit of better atomic clock performance [1,2].

For room-temperature optical lattice clocks (OLCs) based on Yb and Sr, the BBR shift represents the largest uncanceled systematic frequency shift, amounting to -2.4×10^{-15} and -4.8×10^{-15} [3], respectively, while typically also constituting the largest source of uncertainty in these clocks [4,5]. The uncertainty in the BBR shift stems from (i) uncertainty in the BBR environment, specific to the apparatus and assessment techniques, and (ii) uncertainty in the atomic response to BBR, specific to the atomic species. For evaluation purposes, the BBR shift is partitioned into a dominant "static" contribution and a smaller "dynamic" correction [6]. BBR shift uncertainties as low as $\approx 1 \times 10^{-18}$ have been reported for room-temperature Yb and Sr OLCs with the leading uncertainty attributed to the dynamic correction of the atomic response [5–13]. This motivates independent evaluations of the dynamic correction using varied approaches. At the same time, an appealing avenue towards better clock accuracy is to eliminate the need for precise knowledge of the dynamic correction altogether.

At cryogenic temperatures, the BBR shift is highly suppressed. Of more practical significance, however, is that (i) the temperature sensitivity is suppressed, providing greater tolerance to absolute temperature uncertainty and (ii) the uncertainty due to the atomic response is rendered negligible ($< 10^{-21}$) for both Yb and Sr. Despite these clear benefits, cryogenic operation is hindered by the practical needs of clock operation, which include preparing and optically addressing lattice-trapped atoms while maintaining a well-characterized BBR environment.

Cryogenic OLCs have previously been demonstrated in Refs. [14–16]. With two distinct designs, the interrogated atoms are predominantly surrounded by cryogenic surfaces, suppressing the BBR shift. One design relies on shuttling lattice-trapped atoms to a small cryogenic enclosure for interrogation with reduced exposure to external thermal radiation. The other design utilizes a double-layered static shield in which the lattice-trapped atoms are loaded and interrogated. In both designs, however, the atoms retain direct line of sight to external thermal radiation, which

*Contact author: andrew.ludlow@nist.gov

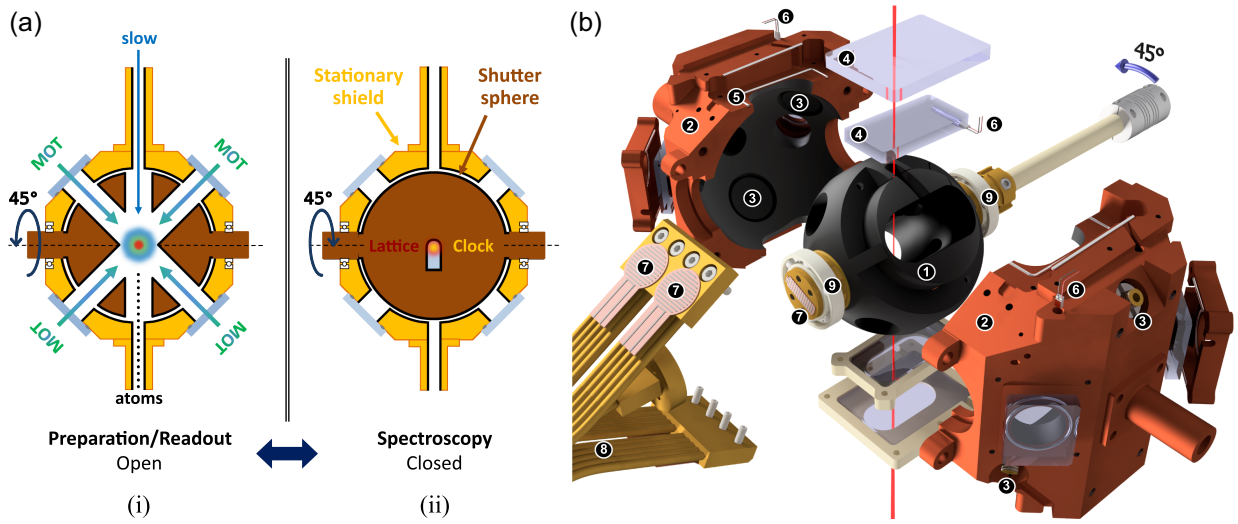

FIG. 1. Illustrations of the shield structure and function. (a) Horizontal cross section at midplane of the shield. (i) Open configuration when the apertures of the shutter sphere (brown) and the stationary shield (gold) are aligned, providing physical and optical access for the atomic beam and the magneto-optical trap (MOT) beams to cool and trap the atoms. After loading the atoms into the vertical optical lattice, the shutter sphere is rotated around the dashed axis, shuttering direct exposure to external thermal radiation. (ii) Closed configuration when clock spectroscopy is performed in a near-ideal BBR environment determined by the controlled shield temperature. A slit on the shutter sphere maintains optical access for the vertical lattice and the copropagating clock spectroscopy beam. (b) Exploded 3D rendering of the shield. The shutter sphere (1), 6 cm in diameter, is shown in the closed configuration for spectroscopy, with its apertures facing the internal surface of the stationary radiation shield (2) and aligned with electrodes for dc Stark evaluation (3). The lattice beam (vertical red line) is permitted through the slit on the sphere, while external thermal radiation is blocked by the double stack of absorptive windows (4) thermally coupled to the shield through pressed indium (5). RTDs are distributed (6) to measure the temperature of the sphere (3×), the two stationary shield halves (4×), and a vertical window with direct line of sight to the atoms during spectroscopy (1×) (only 3 RTDs are shown). Three heater sets (7) control and stabilize the shield temperature. Flexible copper braids (8) to the cryocooler tip accommodate the sphere rotation. All internal copper surfaces are coated with absorptive black coating. Ceramic ball bearings (9) support the sphere inside the shield. An out-of-vacuum stepper motor rotates the sphere between closed and open configurations in ≈100 ms with minimal vibration owing to its balanced design.

contributes significantly to the shift. Residual factors such as reflections within the cryogenic region or transmission through windows must be precisely taken into account. Ultimately, uncertainties associated with these factors lead to BBR shift uncertainties in those cryogenic OLCs that are comparable to what has been achieved with room-temperature OLCs ($\approx 1 \times 10^{-18}$).

In this Letter, we demonstrate a cryogenic ^{171}Yb OLC, achieving a BBR shift uncertainty of 1.7×10^{-20}. Our core strategy is to furnish the interrogated atoms with a near-ideal BBR environment at a cryogenic temperature. Below we describe a BBR enclosure, or "shield," that accomplishes this task by dynamically shuttering all but the necessary optical access for clock spectroscopy. With this design, external thermal radiation is thoroughly extinguished, with its small residual effects bounded through radiation modeling. Conservative uncertainty estimates of the resulting residual shift are then assigned with minimal reliance on the details of the model. Instead, the leading uncertainty is attributed to thermal gradients across the shield, which are evaluated with contact thermometers embedded in the shield components. While the BBR shift uncertainty is minimized at cryogenic temperatures, the shield is also capable of providing near-ideal BBR environments over a wide range of temperatures, from ≈77 K to ≈320 K. This capability facilitates, for the first time in Yb, an independent determination of the leading dynamic BBR correction by direct observation, achieving a level of precision comparable to other methods. Importantly, while our shield is implemented in an Yb OLC, the design is general to all OLC species.

An illustration of the basic function of the shield is shown in Fig. 1(a). The shield consists of a radiation enclosure with a sphere-shaped core, referred to as the "the shutter sphere," that is actuated between an "open" and a "closed" configuration. The open configuration provides access for atomic sample preparation and readout. The closed configuration provides a controlled BBR environment for clock spectroscopy. In the closed configuration, the atoms have no direct exposure to the external environment and are exclusively surrounded by highly emissive surfaces whose temperatures are monitored and controlled in real time. A small vertical optical access is maintained for the lattice and the copropagating clock spectroscopy beam. This optical access—subtending $< 1\%$ of the solid angle around the atoms—is fitted with double-stacked

N-BK7 substrates that block external thermal radiation and are thermally coupled to the shield.

The detailed components of the shield are shown in the 3D exploded rendering in Fig. 1(b). The main body of the shield, machined from copper for high thermal homogeneity, consists of two halves enclosing the shutter sphere. The shutter sphere is mechanically rotated to selectively block all but the optical access required for clock spectroscopy, realizing the open and closed configurations of the shield. The entire assembly is mounted within an ultrahigh vacuum chamber and cooled through a vibration-isolating helium flow cryocooler [17]. To accommodate the mechanical rotation of the shutter sphere, the cold tip is thermally connected to the shield through a group of flexible copper braids.

Several peripheral components and features are critical for the shield's function in maintaining and characterizing its BBR environment. Eight calibrated negative-temperature-coefficient resistance temperature detectors (RTDs) [17] are embedded in strategic locations in the shield as detailed in Fig. 1. These RTDs provide real-time measurement of the absolute temperature and thermal gradients of the shield surfaces that have a direct line of sight to the atoms during spectroscopy. Additionally, a heater film set is attached to each of the three copper body components (shutter sphere and shield halves) to compensate for imbalances between the different thermal loads and cooling powers to which they are exposed. Each set regulates the mean temperature of the attached component to a programmable set point via an independent feedback loop, providing a uniform temperature enclosure for the atoms.

The internal copper surfaces of the shield are coated with an electrically dissipative black coating, contributing to a Faraday enclosure that protects the atoms during spectroscopy from possible stray-charge-induced dc Stark shifts. The apertures on the stationary shield intended for optical access are fitted with N-BK7 optical substrates [pale blue in Fig. 1(a)], which are largely opaque to the external thermal radiation. The apertures for the atomic thermal beam are equipped with high-aspect-ratio tubes to reduce external radiation influx. Both the substrates and the tubes are thermally coupled to the shield through pressed indium, and contribute to the overall external radiation suppression.

A core feature of the shield is its actuated nested design, which effectively attenuates external radiation entering through the apertures. This attenuation occurs through multiple reflections off the highly absorptive black coatings and through the absorption of radiation by the window substrates. As a result, only residual amounts of the radiation ultimately reach the atoms. At 77 K, we estimate an upper bound of 4×10^{-21} on the shift caused by the residual external radiation from all apertures. This assessment is based on a reverse ray-tracing modeling with conservative estimates of both the emissivity of the black coatings and the transmission properties of the window over the whole electromagnetic spectrum [18]. We assign this upper bound as the uncertainty for the residual radiation shift.

TABLE I. BBR shift uncertainty ($\times 10^{-21}$ clock frequency) for Yb2 for three typical mean set temperatures. DLS: direct-line-of-sight.

BBR environment	77.0 K	298.5 K	318.2 K
RTD temperature measurements			
Manufacturer calibration	3.4	580	810
Electronic measurement error	2.2	130	160
Self-heating	< 0.1	1	1
Parasitic conduction and radiation	1	< 1	< 1
Temperature inhomogeneity			
DLS surfaces	16	130	320
Residual external radiation	3	< 1	5
Non-DLS surfaces and others	4	2	30
atomic response			
Static polarizability	0.2	45	60
Dynamic corrections	0.3	940	1380
BBR Zeeman factor	< 0.01	< 1	< 1
Total BBR environment	17	600	890
Total atomic response	0.4	940	1380
Total	17	1120	1640

Another critical feature is the high thermal homogeneity maintained by the internal shield surfaces during spectroscopy, achievable across a wide temperature range from 77 K to 318 K. Despite being constructed from three separate components of bulk copper, setting the mean temperature of each component to a common temperature leads to an overall BBR homogeneity limited by the copper thermal conductivity and the RTD calibration uncertainty. The shield achieves stability and in-loop temperature control at the submillikelvin level for averaging times > 8 s for each component, facilitated by real-time thermal feedback [18]. We utilize the RTD measurements, corroborated with thermal simulations, to capture the thermal extremes of all internal surfaces of the shield with direct line of sight to the atoms [18]. Weighted by the solid angles subtended by those surfaces, we use those temperature extremes to estimate a uniform probability distribution of the induced shift at the atoms. We then assign its standard deviation (1.6×10^{-20}) as the uncertainty on the shift, corresponding to a BBR temperature uncertainty of 29 mK. We perform similar analysis at 298.5 K and 318.2 K. The remaining sources of uncertainty of the BBR shift are detailed in Table I and in Ref. [18].

Electrical insulation is placed between the shield halves to suppress eddy currents during the MOT loading phase, produced by large changes in the vertical magnetic flux. A thin vertical cut in the shutter sphere serves the same function. Three mutually perpendicular pairs of electrodes, thermally coupled to but electrically insulated from the

shield, are positioned to have a direct line of sight to the atoms during spectroscopy. The electrodes, grounded during clock operation, are utilized in dedicated measurements to verify the absence of a dc Stark shift, for example, due to the accumulation of stray static charges.

The cryogenic shield is installed in one of our Yb lattice clock systems, referred to as Yb2. In contrast, our other Yb clocks, Yb1 and YbT, employ room-temperature BBR control solutions. These serve as stable frequency references in the measurements described below. Specifically, Yb1, a laboratory-based clock, utilizes an in-vacuum shield at room temperature that is passively coupled to the vacuum chamber [10]. Meanwhile, YbT, a transportable clock, features a small, temperature-stabilized vacuum chamber that functions as its BBR shield [33]. The three systems share the clock laser, while Yb1 and Yb2 share cooling and lattice lasers. Yb2 alone utilizes an optical enhancement cavity for the lattice.

We first observe the total BBR shift of the Yb clock transition due to room-temperature radiation by performing simultaneous narrow-line spectroscopy with a 560 ms Rabi pulse on Yb2 and Yb1. The Yb2 shield temperature is set at 77.03 K, while the Yb1 shield is at 296.78 K. Line scans and fits shown in Fig. 2(a) reveal a clock shift that is consistent at the 1σ level of the expected BBR shift after accounting for the first-order Zeeman shift in such scans.

By varying the temperature of the Yb2 shield, we apply the BBR shift model

$$\nu_{\mathrm{BBR}}(t) = \nu_{\mathrm{stat}} t^4 + \nu_{\mathrm{dyn},6} t^6 + \nu_{\mathrm{dyn},8} t^8 + \mathcal{O}(t^{10}), \quad (1)$$

to the clock frequencies at five selected Yb2 shield temperatures. Here $t \equiv T/T_0$ is a normalized temperature parameter for a BBR environment characterized by an absolute temperature T, with conventional reference temperature $T_0 = 300$ K. The first term on the right-hand side of Eq. (1) is the static approximation to the BBR shift, while the remaining terms are dynamic corrections that account for the spectral dependence of the atomic polarizabilities and the BBR.

In Fig. 2(b), the Yb2 frequency difference from a reference Yb clock ($\nu_{\mathrm{Yb2}} - \nu_{\mathrm{ref}}$) is plotted as a function of the shield temperature. In this case, the reference Yb clock is either Yb1 or YbT, both corrected for all systematics, while Yb2 is corrected for all systematics except for the BBR shift. Equation (1) is then fit to measurements of the frequency difference at six different temperatures, in this case fixing $\nu_{\mathrm{dyn},6}$ and $\nu_{\mathrm{dyn},8}$ to the established values in the literature [9,10]. The best fit is achieved with the static coefficient $\nu_{\mathrm{stat}} = -1.2545(10)$ Hz. This is in excellent agreement with the more precise measurement by application of a static electric field in Ref. [7] and is self-consistent with the BBR corrections applied to Yb1 and YbT. We note that the fitted value of ν_{stat} maintains good agreement with Ref. [7], regardless of the choice of $\nu_{\mathrm{dyn},6}$, whether it be the value in Ref. [10] or the value reported later in this Letter. The measurement of ν_{stat} here provides a confirmation of the dc differential polarizability of the ^{171}Yb clock transition, establishing an independent verification of the room-temperature static BBR correction at the 2×10^{-18} level.

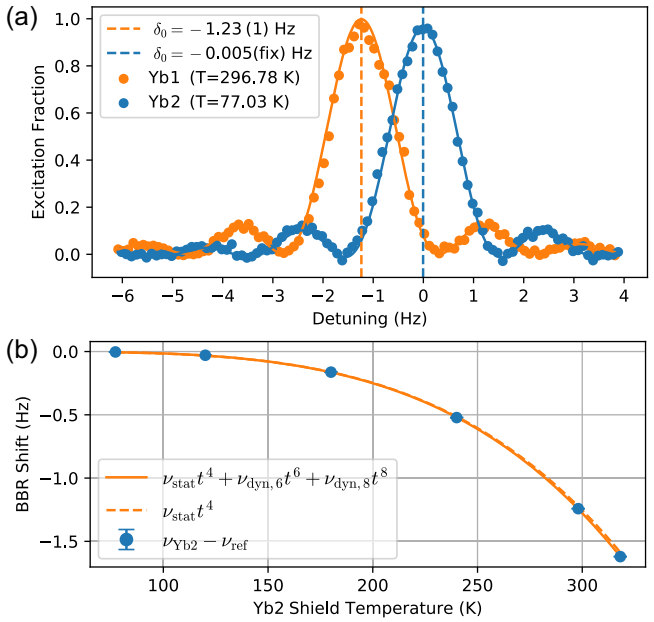

FIG. 2. (a) Average of two simultaneous Rabi line scans on two Yb clocks with the Yb2 shield at cryogenic temperature and the Yb1 shield at room temperature. The solid lines are Rabi lineshape fits with center frequency δ_0. Both scans have been corrected for first order magnetic shifts at the 15 mHz level, with all other corrections well below that. Zero detuning is defined at zero BBR shift relative to Yb2 center frequency. (b) BBR shift of Yb2 as a function of the shield temperature as compared to the reference clock. Both clock frequencies are corrected for all known systematic shifts, except for the BBR shift on Yb2. The solid orange line is the best fit of Eq. (1) with fixed dynamic coefficients. The dashed line represents the static contribution to the BBR shift. The 68% confidence error bars are small compared to the total BBR shift scale.

Armed with the uniform BBR environment provided by the shield from cryogenic to above-room temperatures, we analyze a series of comparisons between the three clocks [34] to determine $\nu_{\mathrm{dyn},6}$. We fit the observed frequency difference, corrected for all systematics except for the first-order dynamic contribution, to a linear model whose slope is $\nu_{\mathrm{dyn},6}$ expressed as

$$\Delta(t_{\mathrm{Yb2}}, t_{\mathrm{ref}}) = \nu_{\mathrm{dyn},6}(t_{\mathrm{Yb2}}^6 - t_{\mathrm{ref}}^6) + \nu_c, \quad (2)$$

where $t_{\mathrm{Yb2}}(t_{\mathrm{ref}})$ is the normalized temperatures of Yb2 (Yb1/YbT) and ν_c accommodates any frequency offset between clock pairs. Most measurements were conducted at Yb2 shield temperatures of 77 K, 298 K, and 318 K, while the reference clocks were close to room temperature.

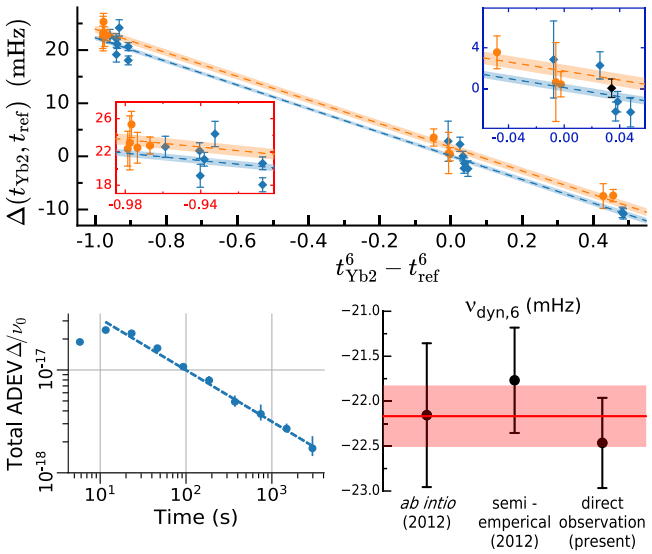

FIG. 3. Top: observed frequency difference between two pairs of Yb clocks: $\Delta(t_{\mathrm{Yb2}}, t_{\mathrm{Yb1}})$ (blue) and $\Delta(t_{\mathrm{Yb2}}, t_{\mathrm{YbT}})$ (orange). Vertical error bars represent combined statistical and differential systematic uncertainties, calculated as explained in the main text. The dashed lines and shaded bands represent the best fit line with slope $\nu_{\mathrm{dyn},6} = -22.47(50)$ mHz. Insets are magnified scales of runs at 77 K (red frame) and 298 K (blue frame) Yb2 shield temperatures. Bottom left: total Allan deviation of a single synchronized run (black diamond in the top subfigure inset) with an estimated instability of $1.10(3) \times 10^{-18}$ fractional frequency at the full measurement time (8000 s). Bottom right: comparison between *ab initio* [9], semiempirical [10], and direct experimental measurement (present work) of $\nu_{\mathrm{dyn},6}$. The red horizontal line represents the weighted mean of the three values, with shaded error band representing the 68% confidence interval.

We performed a global fit to two expanded datasets of 15 measurements of $\Delta(t_{\mathrm{Yb2}}, t_{\mathrm{Yb1}})$ and 10 measurements of $\Delta(t_{\mathrm{Yb2}}, t_{\mathrm{YbT}})$ with a common slope and independent offsets, as shown in Fig. 3. The best fit is achieved with $\nu_{\mathrm{dyn},6} = -22.47(50)$ mHz. The reported uncertainty on the fit is inflated by the square root of the reduced chi squared $\sqrt{\chi^2_{\mathrm{red}}} = \sqrt{1.4}$. The statistical uncertainty for each measurement was determined by the total Allan deviation extrapolating a white noise model to the full measurement time [35]. For about half of the measurements, we interrogated the clocks synchronously to reject common-mode clock laser noise and achieve better differential stability. The total Allan deviation plot of a selected synchronized measurement is also shown, with a white noise fit of $9.9(3) \times 10^{-17}/\sqrt{\tau}$ fractional frequency instability where τ is the averaging time in seconds. For each measurement, we excluded from the differential systematic uncertainty any effects that do not influence the slope. Temperature drift and measurement uncertainty on the abscissa are negligible. However, we investigated temperature-dependent factors, such as the variation of the background gas pressure, which could bias the fitted $\nu_{\mathrm{dyn},6}$ through a correlated background gas collisional shift. The reported uncertainty is inflated to account for the possible bias, as detailed in Ref. [18]. We note that any plausible background gas collisional shift bias is bounded to less than 0.6σ from the reported measurement.

The fitted $\nu_{\mathrm{dyn},6} = -22.47(50)$ mHz in this work is in good agreement with the *ab initio* $\nu_{\mathrm{dyn},6} = -22.16(80)$ mHz [9] and semiempirical $\nu_{\mathrm{dyn},6} = -21.77(59)$ mHz [10] previously reported in the literature for Yb using entirely different methods [36]. We thus report the weighted mean of the three determinations at $\nu_{\mathrm{dyn},6} = -22.17(34)$ mHz, with 30% reduced uncertainty compared to the combined uncertainty of the previous two values.

In summary, we describe the design and operation of a cryogenic radiation shield that realizes an unprecedented BBR Stark shift uncertainty of 1.7×10^{-20} in an Yb OLC. The shield realizes such control by thoroughly rejecting external thermal radiation and enclosing the clock atoms from all 4π steradians by emissive and thermally uniform surfaces, creating a near-ideal cryogenic BBR environment during clock spectroscopy. Additionally, by modulating the shield temperature, we directly measure the BBR static and leading dynamic coefficients at the 2×10^{-18} and 1×10^{-18} levels, respectively. This reduces the latter's literature-combined uncertainty by 30%, an improvement that is particularly valuable for enhancing the accuracy of Yb OLCs operated at room temperature.

Acknowledgments—We thank Jeffrey A. Sherman and Vladislav Gerginov for their careful reading of the manuscript and their critical feedback. We also thank Kyungtae Kim, Dahyeon Lee, and Jun Ye for providing cryogenic silicon cavity stable reference [37] to our clock laser during a subset of the measurements in this work, as well as Nicholas V. Nardelli and Tara Fortier for operating the optical frequency comb that enabled this stability transfer. We wish to express our gratitude to Elizabeth A. Donley for her service as the NIST Time and Frequency Division Chief over the past several years. We gratefully acknowledge funding support from NIST, the Office of Naval Research, National Science Foundation QLCI Grant No. 2016244, and by an appointment to the Intelligence Community Postdoctoral Research Fellowship Program at NIST administered by ORISE through an interagency agreement between the U.S. DoE and the Office of the Director of National Intelligence.

Y. S. H. led the design, assembly, and integration of the shield into Yb2, as well as its operation. K. B. and A. D. L. contributed to the design. Y. S. H., K. B., and J. L. S. jointly conducted the analysis. T. K. and K. B. contributed to the shield integration into the clock. T. G. was responsible for the maintenance of the optical local oscillators. The operation of Yb1 was handled by J. L. S. and B. D. H., while E. W. S., R. C. B., T. R., T. B., and A. I. H. operated

YbT. The project was conceptualized by K. B. and A. D. L., who also supervised the entire project. All authors contributed to the final manuscript and discussed the results and the analysis.

The authors declare no competing interests.

Data availability—The data that support the findings of this Letter are not publicly available. The data are available from the authors upon reasonable request.

[1] W. M. Itano, L. L. Lewis, and D. J. Wineland, Shift of $^2S_{\frac{1}{2}}$ hyperfine splittings due to blackbody radiation, Phys. Rev. A **25**, 1233 (1982).

[2] A. D. Ludlow, M. M. Boyd, J. Ye, E. Peik, and P. O. Schmidt, Optical atomic clocks, Rev. Mod. Phys. **87**, 637 (2015).

[3] Shifts and uncertainties given without units are in fractional units of the respective clock frequency.

[4] W. F. McGrew, X. Zhang, R. J. Fasano, S. A. Schäffer, K. Beloy, D. Nicolodi, R. C. Brown, N. Hinkley, G. Milani, M. Schioppo, T. H. Yoon, and A. D. Ludlow, Atomic clock performance enabling geodesy below the centimetre level, Nature (London) **564**, 87 (2018).

[5] A. Aeppli, K. Kim, W. Warfield, M. S. Safronova, and J. Ye, Clock with 8×10^{-19} systematic uncertainty, Phys. Rev. Lett. **133**, 023401 (2024).

[6] K. Beloy, N. Hinkley, N. B. Phillips, J. A. Sherman, M. Schioppo, J. Lehman, A. Feldman, L. M. Hanssen, C. W. Oates, and A. D. Ludlow, Atomic clock with 1×10^{-18} room-temperature blackbody Stark uncertainty, Phys. Rev. Lett. **113**, 260801 (2014).

[7] J. A. Sherman, N. D. Lemke, N. Hinkley, M. Pizzocaro, R. W. Fox, A. D. Ludlow, and C. W. Oates, High-accuracy measurement of atomic polarizability in an optical lattice clock, Phys. Rev. Lett. **108**, 153002 (2012).

[8] T. Middelmann, S. Falke, C. Lisdat, and U. Sterr, High accuracy correction of blackbody radiation shift in an optical lattice clock, Phys. Rev. Lett. **109**, 263004 (2012).

[9] M. S. Safronova, S. G. Porsev, and C. W. Clark, Ytterbium in quantum gases and atomic clocks: Van der Waals interactions and blackbody shifts, Phys. Rev. Lett. **109**, 230802 (2012).

[10] K. Beloy, J. A. Sherman, N. D. Lemke, N. Hinkley, C. W. Oates, and A. D. Ludlow, Determination of the $5d6s\ ^3D_1$ state lifetime and blackbody-radiation clock shift in Yb, Phys. Rev. A **86**, 051404(R) (2012).

[11] M. S. Safronova, S. G. Porsev, U. I. Safronova, M. G. Kozlov, and C. W. Clark, Blackbody-radiation shift in the Sr optical atomic clock, Phys. Rev. A **87**, 012509 (2013).

[12] Ch. Lisdat, S. Dörscher, I. Nosske, and U. Sterr, Blackbody radiation shift in strontium lattice clocks revisited, Phys. Rev. Res. **3**, L042036 (2021).

[13] M. Heo, H. Kim, D. Yu, W. Lee, and C. Y. Park, Evaluation of the blackbody radiation shift of an Yb optical lattice clock at KRISS, Metrologia **59**, 055002 (2022).

[14] I. Ushijima, M. Takamoto, M. Das, T. Ohkubo, and H. Katori, Cryogenic optical lattice clocks, Nat. Photonics **9**, 185 (2015).

[15] M. Takamoto, I. Ushijima, M. Das, N. Nemitz, T. Ohkubo, K. Yamanaka, N. Ohmae, T. Takano, T. Akatsuka, A. Yamaguchi, and H. Katori, Frequency ratios of Sr, Yb, and Hg based optical lattice clocks and their applications, C.R. Phys. **16**, 489 (2015).

[16] R. Schwarz, A cryogenic strontium lattice clock, PhD thesis, Gottfried Wilhelm Leibniz Universität, 2022.

[17] The closed cycle cryocooler is a custom split-flow design based on the ColdEdge Stinger, specified at an estimated cooling power of 5 W at 50 K. Lakeshore provides the negative-temperature-coefficient RTDs (Cernox CX-1080-SD-HT) whose calibrations are NIST-traceable. The RTDs are paired with a Lakeshore model 336 cryogenic temperature controller for temperature readout and thermal feedback. Specification of commercial products is for informational purposes only. This does not imply recommendation or endorsement of any commercial product by NIST, nor does it imply that the products identified are necessarily the best available for the experimental purposes.

[18] See Supplemental Material at http://link.aps.org/supplemental/10.1103/4tky-jmsm, which includes Refs. [19–32], for additional details about the shield, its operation, and the BBR shift evaluation and uncertainty analysis.

[19] A. K. A. Al-Masoudi, A strontium lattice clock with reduced blackbody radiation shift, Ph.D thesis, Hannover: Gottfried Wilhelm Leibniz Universität Hannover, 2016.

[20] Md. S. Islam, C. M. B. Cordeiro, Md. J. Nine, J. Sultana, A. L. S. Cruz, A. Dinovitser, B. Wai-Him Ng, H. Ebendorff-Heidepriem, D. Losic, and D. Abbott, Experimental study on glass and polymers: Determining the optimal material for potential use in terahertz technology, IEEE Access **8**, 97204 (2020).

[21] M. Naftaly and R. E. Miles, Terahertz time-domain spectroscopy for material characterization, Proc. IEEE **95**, 1658 (2007).

[22] A. Adibekyan, E. Kononogova, C. Monte, and J. Hollandt, High-accuracy emissivity data on the coatings Nextel 811-21, Herberts 1534, Aeroglaze Z306 and Acktar fractal black, Int. J. Thermophys. **38**, 89 (2017).

[23] J. Ekin, *Experimental Techniques for Low-Temperature Measurements: Cryostat Design, Material Properties and Superconductor Critical-Current Testing* (Oxford University Press, New York, 2006).

[24] J. G. Hust, Thermal anchoring of wires in cryogenic apparatus, Rev. Sci. Instrum. **41**, 622 (1970).

[25] J. W. Farley and W. H. Wing, Accurate calculation of dynamic Stark shifts and depopulation rates of Rydberg energy levels induced by blackbody radiation. Hydrogen, helium, and alkali-metal atoms, Phys. Rev. A **23**, 2397 (1981).

[26] S. G. Porsev and A. Derevianko, Multipolar theory of blackbody radiation shift of atomic energy levels and its implications for optical lattice clocks, Phys. Rev. A **74**, 020502(R) (2006).

[27] T. Bothwell, B. D. Hunt, J. L. Siegel, Y. S. Hassan, T. Grogan, T. Kobayashi, K. Gibble, S. G. Porsev, M. S.

Safronova, R. C. Brown *et al.*, Lattice light shift evaluations in a dual-ensemble Yb optical lattice clock, Phys. Rev. Lett. **134**, 033201 (2025).
[28] J. Lodewyck, M. Zawada, L. Lorini, M. Gurov, and P. Lemonde, Observation and cancellation of a perturbing dc stark shift in strontium optical lattice clocks, IEEE Trans. Ultrason. Ferroelectr. Freq. Control **59**, 411 (2012).
[29] J. L. Siegel, W. F. McGrew, Y. S. Hassan, C.-C. Chen, K. Beloy, T. Grogan, X. Zhang, and A. D. Ludlow, Excited-band coherent delocalization for improved optical lattice clock performance, Phys. Rev. Lett. **132**, 133201 (2024).
[30] Y. S. Hassan, T. Kobayashi, T. Bothwell, J. L. Seigel, B. D. Hunt, K. Beloy, K. Gibble, T. Grogan, and A. D. Ludlow, Ratchet loading and multi-ensemble operation in an optical lattice clock, Quantum Sci. Technol. **9**, 045023 (2024).
[31] G. K. White and S. J. Collocott, Heat capacity of reference materials: Cu and W, J. Phys. Chem. Ref. Data **13**, 1251 (1984).
[32] T. L. Nicholson, S. L. Campbell, R. B. Hutson, G. E. Marti, B. J. Bloom, R. L. McNally, W. Zhang, M. D. Barrett, M. S. Safronova, G. F. Strouse *et al.*, Systematic evaluation of an atomic clock at 2×10^{-18} total uncertainty, Nat. Commun. **6**, 6896 (2015).
[33] W. Brand *et al.*, Uncertainty and reproducibility evaluation of a tranportable Yb optical lattice clock (unpublished).
[34] J. L. Siegel *et al.* Comparison of three optical lattice clocks at $\leq 4 \times 10^{-18}$ agreement (unpublished).
[35] Three data points reached the noise floor at $\sim 5 \times 10^{-18}$. For these points, we assigned the floor level as the uncertainty.
[36] The value reported in Ref. [9] is the sum $\nu_{\mathrm{dyn},6} + \nu_{\mathrm{dyn},8} = -22.900(800)$ mHz. We subtract $\nu_{\mathrm{dyn},8} = -0.744(20)$ mHz in Ref. [10] to yield the displayed value $\nu_{\mathrm{dyn},6} = -22.156(800)$. The error on the displayed value is minimally affected by the subtraction, and thus its independence as an *ab initio* calculation of $\nu_{\mathrm{dyn},6}$ is preserved.
[37] E. Oelker, R. B. Hutson, C. J. Kennedy, L. Sonderhouse, T. Bothwell, A. Goban, D. Kedar, C. Sanner, J. M. Robinson, G. E. Marti *et al.*, Demonstration of 4.8×10^{-17} stability at 1 s for two independent optical clocks, Nat. Photonics **13**, 714 (2019).
[38] K. Beloy, X. Zhang, W. F. McGrew, N. Hinkley, T. H. Yoon, D. Nicolodi, R. J. Fasano, S. A. Schäffer, R. C. Brown, and A. D. Ludlow, Faraday-shielded dc Stark-shift-free optical lattice clock, Phys. Rev. Lett. **120**, 183201 (2018).

End Matter

As mentioned in the main text, the shield functions as a Faraday enclosure around the atoms. To verify the absence of any dc Stark shift from stray electric fields, we utilize three pairs of electrodes exposed to the atoms in the closed configuration. These electrodes are arranged to generate controlled electric fields in three nominally mutually orthogonal directions to assess and constrain the dc Stark shift at the atoms' location. Following Ref. [38], we constrain the dc Stark shift in the grounded configuration to $< 10^{-19}$ [18]. Tighter constraints should be readily attainable, if deemed necessary for future clock operation.